Surface Structure Elucidation

DOI: 10.1002/anie.201000910

Real-Space Observation of Surface Termination of a Complex Metal Oxide Catalyst**

*Wei Zhang, Annette Trunschke, Robert Schlögl, and Dangsheng Su**

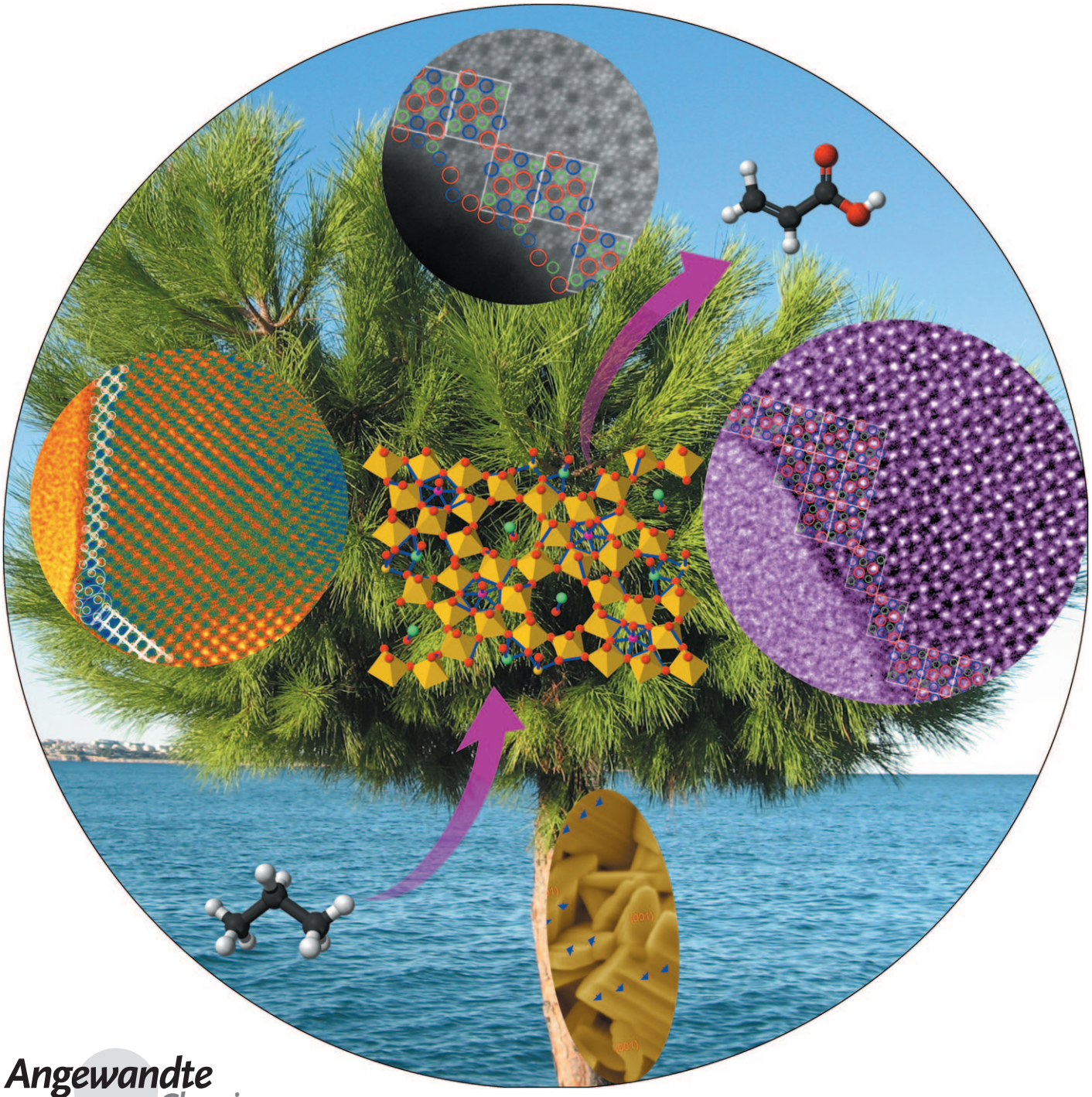

Metal oxides constitute a large class of systems with important applications, some of which depend critically[1–3] on their surface structure. Obtaining this information as average translational termination, even for binary oxides,[4–8] is a difficult task requiring the use of model systems and surface-science techniques.[9–11] Symmetry breaking at the surface of a binary oxide frequently results in strong relaxations and surface structures that are chemically different[5,6,12–14] from cuts through the bulk structure.[15] A case study is the surface of V_2O_5.[16–19] Vanadium oxide is directly relevant[20,21] to catalytic applications in selective oxidation. Variable oxidation states,[17] clusters,[21,22] and amorphous components[23–25] were identified as locations of catalytic activity, none of which are elements of the translational structure. Furthermore, the surface structure[26,27] has been proven to be highly dynamic in termination depending on the nature of adsorbed molecules or atoms.[28–30] The occurrence of covalent[29] vanadyl groups[12] that break the lattice symmetry, or of defects from "lattice oxygen,"[22,31] and the massive surface relaxation upon slight bulk reduction[32] are excellent examples of the complexity[33] of these supposedly simple systems characterized by close-packed bulk structures, which at first glance offer only limited options for restructuring.

Modern high-resolution electron microscopy techniques[34] can be used to complement surface diffraction and scanning probe methods[35] for revealing in real space the local and defective structure of oxide surfaces carrying chemically reactive sites. Despite the enormous progress that TEM has made in imaging inner surfaces and bulk structures of oxides,[36–38] it remains a significant challenge[39–41] to identify the outermost atomic layers of metal oxides. Herein we describe an imaging strategy that focuses on the essential aspects of termination without the need for high-end instrumentation. In nondense structures, multiple possibilities[33] with similar surface energies exist to terminate the structure by breaking bonds within the unit cell. The stabilities of metal–oxygen bonds limit the tendency for relaxation to the extent of forming amorphous rims[24,42] on crystalline bulk structures; thus a distribution of termination modes that change from unit cell to unit cell may exist, giving rise in the TEM projection image to the impression of amorphous[23,25,43] surface layers despite well-structured local terminations.

Many multicomponent metal oxides with large unit cells are nondensely packed three-dimensional structures that can be described formally as stacked two-dimensional arrays of metal oxygen polyhedra, with free space aggregating to channel structures upon stacking. The basic structural units are thus slabs of two-dimensional assemblies of polyhedra, large enough to represent a minimum set of channels occurring as holes in the slabs. An example is the M1 structure. M1 is the essential crystalline phase in MoVTeNb oxide catalysts that enable the selective oxidation of alkanes, for example the conversion of propane to acrylic acid.[44,45] With a space group of *Pba2* ($a = 21.134$, $b = 26.658$, $c = 4.015$ Å; $\alpha = \beta = \gamma = 90°$), the M1 phase consists of a complex network of $(Mo,V,Nb)O_6$ octahedra grouped around pentagonal bipyramidal oxo clusters to form a nondensely arranged slab of 0.4 nm thickness. A representation of the slab that forms the basic structural unit of the M1 structure is shown in Figure 1a. This slab coincides with the crystallographic unit

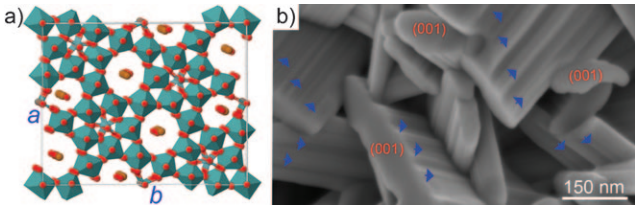

Figure 1. Crystallographic model of the M1 phase and morphology of M1. a) Unit cell along the ⟨001⟩ direction. b) High-resolution SEM image of M1 particles. Blue arrows indicate the ⟨001⟩ direction.

cell that is used as a model to describe the arrangement of atoms in a suitable way for crystallographic analysis. These slabs are stacked through metal–oxygen bonds along the ⟨001⟩ direction to form cylindrical crystals (Figure 1b).[46] Along the long axis of the cylinders, a pattern of hexagonal, heptagonal, and pentagonal channels terminating in the (001) plane (see Figure 1a) creates an overall nondense structure with strongly anisotropic nominal termination modes at the basal (001) and {hk0} prismatic faces (Figure 1b).[47] Niobium predominantly occupies the pentagonal bipyramidal positions, whereas nonstoichiometric amounts of tellurium oxo units populate the hexagonal and heptagonal channels. Buttrey and co-workers worked out the complex crystallographic model of the M1 phase using aberration-corrected high-resolution STEM techniques.[48] This analysis gives an excellent and detailed insight into the crystal chemistry of the phase. It falls short, however, of addressing the issue of termination. The presence of multiple steps on the by far prevalent prismatic faces[46,49,50] is an indication of how unlikely it is that the structure will terminate in a single low-energy configuration, as exemplified[51] in the much simpler structure of titania, for which faceting was found to be critical for reactivity. It is customary in the literature to assign the minority (001) faces as the active sites,[52,53] as there the bulk crystal structure of M1 is assumed to terminate without restructuring. Catalytic experiments trying to verify this assumption gave conflicting results[50,54,55] and do not confirm the expected unique role of the (001) faces for catalytic function.

High-resolution (HR) TEM is a tool for obtaining real-space structural information about nontranslational symmetry as well as on the average crystal structure. For our routine

[*] Dr. W. Zhang, Dr. A. Trunschke, Prof. Dr. R. Schlögl, Dr. D. Su
Department of Inorganic Chemistry
Fritz Haber Institute of the Max Planck Society
Faradayweg 4–6, 14195 Berlin (Germany)
Fax: (+49) 30-8413-4401
E-mail: dangsheng@fhi-berlin.mpg.de
Homepage: http://www.fhi-berlin.mpg.de

[**] The work was supported by the SFB 546. We thank T. Wolfram for providing the sample. L. Yao, L. Shao, J. Rao, B. Zhu, B. Zhang, H. Sauer, and Q. Zhang are gratefully acknowledged for the stimulating discussions.

Supporting information for this article is available on the WWW under http://dx.doi.org/10.1002/anie.201000910.

CM200-LaB6 TEM instrument, the point resolution near Scherzer focus (e.g. 3.0 Å at defocus $\Delta f = -10$ nm) approaches the resolution at Scherzer focus (2.4 Å at $\Delta f = -71$ nm), while it becomes more reduced for extreme values of Δf, for example 17 Å at $\Delta f = -1150$ nm and 16 Å at $\Delta f = 1000$ nm, as illustrated by the contrast transfer functions (CTF) in Figure S1 in the Supporting Information. We propose to vary the CTF upon analyzing the termination. The atomic structure information can be complemented on the one hand by the identification of the supramolecular unit cell disposition, for example 21 Å × 26 Å of M1 phase along ⟨001⟩, and on the other hand by the termination of the unit cells at the surface without carrying the atomic information.

Figure 2a shows such a unit cell disposition image for M1 along ⟨001⟩. The simulated images (see the insets) are consistent with their experimental counterpart using crystallographic models with and without Te in heptagonal channels.[46] It is important to note that this image does not represent "unit cells" as models in crystallographic considerations but rather shows the border lines of the basic structural units representing locations of high density of metal oxygen polyhedra (see also Figure 1a). The letters A, B, and C in Figure 2a indicate areas of slight variations in contrast and orientation of the unit cells. It is assumed[47] that a variation in the location of Te between the hexagonal and heptagonal channels is responsible for this local variation in geometry, as indicated by the slight modification of the shape of the individual representations of heptagonal channels (elongated vs. spherical for filled or empty channels, clearly visible also in the simulation insets of Figure 3). The differences between C and A are due to the variations in their thickness and orientation. The gray "termination line" (D) is an imaging artifact and can be discriminated from a real structure by its strong variation with focus conditions.

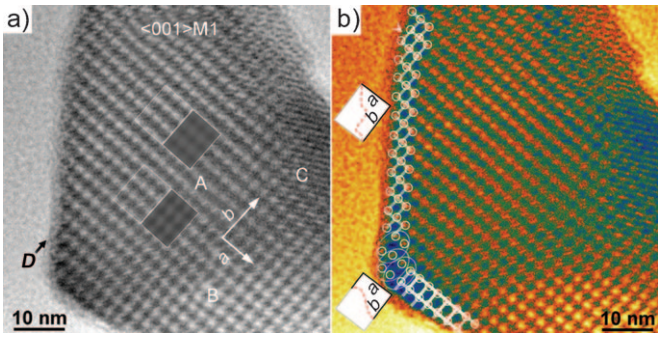

Figure 2. HR-TEM images of one M1 particle along the ⟨001⟩ direction far from Scherzer focus. a) The image in grayscale and b) its counterpart displayed in color mode (temperature style, where the color settings are based on the contrast variation) using Gatan DigitalMicrograph software. The bottom and top insets in (a) are the corresponding simulated lattice images using crystallographic models with and without Te occupying heptagonal channels, respectively. Both are conditioned at a thickness of 28.9 nm and $\Delta f = -1150$ nm. In (b), the perimeter of the M1 particle is highlighted. The left two rectangles are schematic illustrations of fractured structural units in the left and bottom-left perimeters. The termination indicated by the arrow is similar to that in the bottom.

Figure 2b shows the false-color representation of the perimeter of a M1 particle. The termination occurs through breaks in basic structural units, which form the prismatic surface of the needle that is imaged in the projection along ⟨001⟩. Two break lines connecting the channel systems in different ways are indicated in the small schematic representations of the basic structural units in Figure 2b. These terminations break the crystal periodicity in the bulk and create two chemically inequivalent forms of the prismatic faces. The consequence is a termination consisting of roughly half-pipes of the formerly closed channels and of wall fragments exposing the thinnest sections through the mesh of polyhedra.

The false-color representation of the (001) surface (Figure 2b) reveals the variation in sample thickness that leads to a varying representation of the contrast of the bulk unit cells. The complexity of the termination is further enhanced by the situation at the apex of the particle, where two columns of unit cells indicated by the ellipsoids in Figure 2b exhibit a strong local relaxation with a modified channel structure.

Figure 3 shows the projection of the prismatic face of a different M1 particle. This image was taken with a CTF close to the Scherzer focus, thus allowing projection of all metal oxygen polyhedra and the channel structure as expected from the crystallographic model of M1. The bottom inset shows the same situation imaged with the unit cell CTF used also for

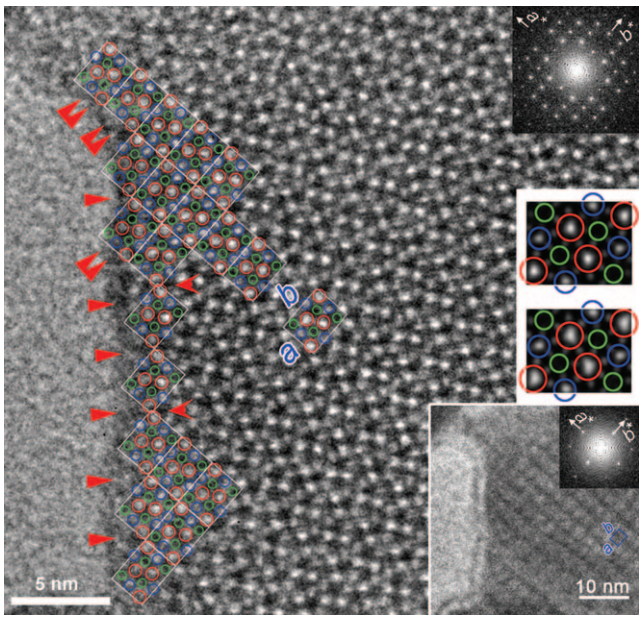

Figure 3. HR-TEM image of one M1 particle along the ⟨001⟩ direction near Scherzer focus. The top-right inset shows the fast Fourier transform (FFT). The bottom-right inset corresponds to the image and the FFT far from Scherzer focus and shows the unit cell information (rectangle). The right two insets are the simulated images (conditioned at a thickness of 13.2 nm and $\Delta f = -10$ nm) as well as their underlying heptagonal (red), hexagonal (blue), and pentagonal (green) channels using crystallographic models with (top) and without (bottom) Te occupying heptagonal channels. The arrows and double arrows indicate the aforementioned two termination breaks. There are some matching residues among unit cells adjacent to the perimeter, as indicated by the stealth arrows.

Figure 2. The top inset gives the fast Fourier transform of the object, which is in full agreement with the crystallographic structure and is further used to verify the exact orientation of the needle along the electron-beam axis. The terminating fragments are better resolved owing to the more suitable CTF, whereas the basic structural units are hard to recognize without the schematic representations. The surface morphology is the same as on the long side of the particle in Figure 2. The arrows in Figure 3 designate channel features that are much weaker than in the bulk owing to imaging artifacts at the boundary of a periodic object and to incomplete channel walls. It can be seen that the outermost feature visible in Figure 3 is always a bright dot representing a channel structure. Below the surface in the second row, only ordered unit cells of a well-developed crystal can be found, thus illustrating clearly that the complex surface termination is not related to bulk disorder.

Figure S2 in the Supporting Information illustrates the structural consequences of unrelaxed fractured basic structural units, which constitute the surface of the M1 mixed oxide. The top two schemes (Figure S2 a, b in the Supporting Information) relate the splitting of the unit cells and represent the atomic details of the surface derived from the bulk crystallographic structure. In comparison to Figure S2 c, it can be seen that the effective surface area is increased over a hypothetical surface termination with intact basic structural units. The resulting half-pipes, now exposing the former inner surface of the channels, probably run along all prismatic faces, as indicated by the stepped surface morphology seen in the HR-SEM image (Figure 1). The STEM images shown in Figure 4 and Figure S3 in the Supporting Information were recorded on an aberration-corrected instrument to confirm the termination mechanism discussed above.

The surface is terminated with the opened heptagonal and hexagonal channels. A consequence of this termination is the liberation of tellurium oxo groups that are no longer contained in the channels but can freely disperse over the whole surface. This consequence of the terminating mechanism explains the well-documented fact that tellurium is in large excess over all other elements at the surface of the working catalyst investigated with depth-resolved X-ray photoelectron spectroscopy.[56]

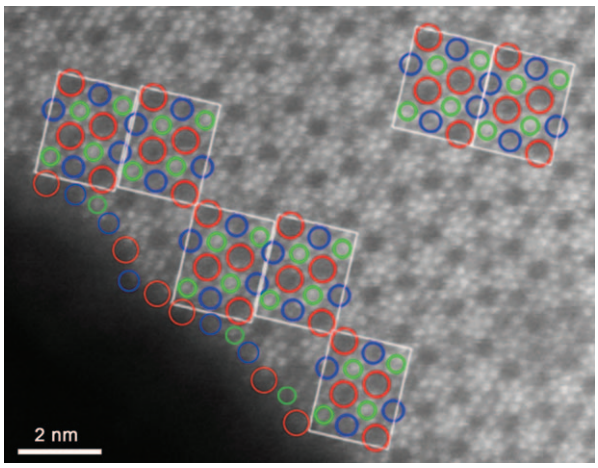

Figure 4. STEM image of one M1 particle along the ⟨001⟩ direction. The surface was partially highlighted by the characteristic channels (heptagonal, hexagonal, and pentagonal) of the M1 phase. The bright dots represent columns of M–O polyhedra.

The simulations of the atomic surface structures of the two terminations displayed in Figure S2 d, e in the Supporting Information reveal clearly that this termination mode exposes corners of metal oxygen polyhedra to the outer surface that would not be accessible by reactants and adsorbing molecules on a surface made of intact unit cells. The element coding of the structure simulation represented in Figure S2 f, g shows that the fractured terminations expose rows of molybdenum or vanadium atoms with bridging oxygen atoms. Learning from the termination dynamics discussed in the introduction, it can be assumed that all terminal M–O bonds will relax to M=O, and thus double rows of bridging and terminating M–O motifs will become exposed. Alternating M-O-M bridges involve Nb as one end and thus give rise to MoVMoV or MoVNb structures. Such double rows that present coordinatively unsaturated M–O polyhedra to reactants are excellent candidates for active sites performing the dual function of activating and oxidizing adsorbed hydrocarbons. It is most significant that similar local arrangements of polyhedra with terminal and bridging oxygen atoms and an intimate mixture of polyvalent cations in neighboring polyhedra were assigned as active sites situated on the basal planes of the M1 crystals.[53] The terminating mechanism detected in Figure 2 removes the fundamental structural anisotropy of the perfect M1 crystals and thus can explain the conflicting results in the literature about the location of active sites.[50,55] According to the present termination model, we would find active sites of the kind discussed in the literature on all external surfaces of the M1 crystals. It remains unclear whether the relative arrangement of these double rows is convex or concave (like active-site pockets in biological catalysts).

In Figure S4 in the Supporting Information, we seek to explain the average mesostructure of the termination of prismatic faces of the complex M1 oxide. From the SEM image (Figure 1) and the TEM projections in Figure 2 and Figure 3, it appears that most of the surface would exhibit no order but rather present the typical "amorphous surface". Only rarely do the SEM images show stepped structures indicating a regular stacking of microfacets from fractured basic structural units. The schematic representation of the stacking sequence of several-layer slabs of the M1 structure explains both morphological observations. As shown in the left part of Figure S4 b, regular stacking of similar fractured basic structural units leads to the formation of a microfacet with a step structure. The scheme at the right hand side of Figure S4 b assumes a changing termination mode in every layer and shows clearly that regular stacking of such terminations does not lead to supramolecular ordering and hence precludes the observation of the surface morphology. It is the local variation of cationic composition, possibly together with the filling factor of the channels with TeO_x units (causing strain in the channels), that results in a fluctuation of the termination modes. In the absence of large local variations of the metal–oxygen bonds owing to their strong covalent character, the variation in local cationic

composition and hence local charge from dangling bond strengths is the only possibility for the system to minimize its surface free energy. The distribution of the termination structures along a stack of two-dimensional slabs in a cylindrical crystal results in an additive projection in the "amorphous" representation of the surface, viewed along the *c* axis. The impression of amorphousness is an imaging artifact, as neither the local structure nor the supporting bulk crystalline structures are disordered on a local scale.

The combined information allows identification of the termination mode in covalent solids with large unit cells. Termination is achieved by fracturing basic structural units along weak features. Only limited local relaxation may occur, such as conversion of terminal M–O bonds into M=O bonds. The exact fracture line may vary between individual basic structural units with their compositional fluctuation (phase width). The resulting termination will be substantially different from an assumed termination along low-indexed planes of basic structural units. Details of the synthesis kinetics leading to a distribution of cation positions and hence to a fluctuation of bond strengths will control the exact surface morphology. The termination mode is consistent with a perfectly ordered bulk structure that gives, however, no indication of the surface structure.

In the special case of the M1 phase it is explained how termination modes lift the expected structural anisotropy of basal and prismatic surfaces of an anisotropic bulk structural arrangement. In this way it can be expected that reactive sites exist on all orientations of the anisotropic faces of the nondensely packed M1 crystals. In a broader sense, it becomes clear why complicated crystal structures such as M1 are lead structures for attractive catalysts. Covalently bonded and rigid metal oxygen polyhedra in nondense arrangements allow, through the fracturing of their interconnections, the creation of highly exposed metal oxo clusters with coordinatively unsaturated metal sites and with the formation of M=O groups as relaxation products. The combination of bridging and terminal oxygen species allows for the co-existence of nucleophilic and electrophilic oxygen, as required to perform activation and oxidation of hydrocarbons.

In summary, an imaging strategy for surfaces is described that involves adjusting the CTF of the instrument to either atomic details of individual basic structural units or to the supramolecular assembly of basic structural units that form the crystal. The imaging strategy can be applied to other problems in materials science involving structures with large unit cells and does not require special high-end instrumentation.

Experimental Section

Highly crystalline phase-pure M1 phase, confirmed by X-ray analysis, was synthesized by a hydrothermal method.[50] The morphology of the M1 phase was studied by a Hitachi S4800 scanning electron microscope operated at 2 kV. The chemical compositions of the M1 catalyst is (65.6 ± 0.5) at.% Mo, (16.5 ± 0.6) at.% V, (6.7 ± 0.3) at.% Te, and (11.3 ± 0.4) at.% Nb, as determined by energy-dispersive X-ray spectroscopy. A Philips CM200-LaB6 transmission electron microscope operated at 200 kV was employed to investigate the structure of the M1 phase using HR-TEM. The specimens for TEM observation were dispersed in ethanol and deposited on a holey carbon grid. The spherical coefficient of the microscope is $C_s = 1.35$ mm and the chromatic coefficient is $C_c = 1.20$ mm. The Scherzer focus is $\Delta f = -71$ nm with a point resolution of 2.4 Å. The energy spread of the beam is 1.50 eV. Image simulation was performed using JEMS software (copyright P. A. Stadelmann, EPFL, Switzerland) based on the multislice method. An FEI aberration-corrected Titan 80-300 microscope was employed to acquire scanning transmission electron microscopy (STEM) images. The spatial resolution is 1.4 Å in HAADF-STEM mode.

Received: February 12, 2010
Published online: June 22, 2010

Keywords: electron microscopy · heterogeneous catalysis · solid-state structures · structure elucidation · surface chemistry

[1] G. Ertl, *Angew. Chem.* **2008**, *120*, 3578; *Angew. Chem. Int. Ed.* **2008**, *47*, 3524.
[2] X. W. Xie, Y. Li, Z. Q. Liu, M. Haruta, W. J. Shen, *Nature* **2009**, *458*, 746.
[3] J. Biener, A. Wittstock, L. A. Zepeda-Ruiz, M. M. Biener, V. Zielasek, D. Kramer, R. N. Viswanath, J. Weissmüller, M. Bäumer, A. V. Hamza, *Nat. Mater.* **2009**, *8*, 47.
[4] A. Barbier, C. Mocuta, H. Kuhlenbeck, K. F. Peters, B. Richter, G. Renaud, *Phys. Rev. Lett.* **2000**, *84*, 2897.
[5] K. S. Tanwar, S. C. Petitto, S. K. Ghose, P. J. Eng, T. P. Trainor, *Geochim. Cosmochim. Acta* **2008**, *72*, 3311.
[6] J. G. Catalano, C. Park, Z. Zhang, P. Fenter, *Langmuir* **2006**, *22*, 4668.
[7] R. M. Jaeger, H. Kuhlenbeck, H. J. Freund, M. Wuttig, W. Hoffmann, R. Franchy, H. Ibach, *Surf. Sci.* **1991**, *259*, 235.
[8] H. Ibach, *Physics of surfaces and Interfaces*, Springer, Berlin, **2006**.
[9] H. J. Freund, *Angew. Chem.* **1997**, *109*, 444; *Angew. Chem. Int. Ed. Engl.* **1997**, *36*, 452.
[10] M. Bäumer, H. J. Freund, *Prog. Surf. Sci.* **1999**, *61*, 127.
[11] X. Q. Gong, A. Selloni, M. Batzill, U. Diebold, *Nat. Mater.* **2006**, *5*, 665.
[12] C. Kolczewski, K. Hermann, S. Gulmond, H. Kuhlenbeck, H. J. Freund, *Surf. Sci.* **2007**, *601*, 5394.
[13] A. Barbieri, W. Weiss, M. A. Vanhove, G. A. Somorjai, *Surf. Sci.* **1994**, *302*, 259.
[14] M. Ritter, W. Weiss, *Surf. Sci.* **1999**, *432*, 81.
[15] X. G. Wang, W. Weiss, S. K. Shaikhutdinov, M. Ritter, M. Petersen, F. Wagner, R. Schlögl, M. Scheffler, *Phys. Rev. Lett.* **1998**, *81*, 1038.
[16] M. Conte, G. Budroni, J. K. Bartley, S. H. Taylor, A. F. Carley, A. Schmidt, D. M. Murphy, F. Girgsdies, T. Ressler, R. Schlögl, G. J. Hutchings, *Science* **2006**, *313*, 1270.
[17] G. W. Coulston, S. R. Bare, H. Kung, K. Birkeland, G. K. Bethke, R. Harlow, N. Herron, P. L. Lee, *Science* **1997**, *275*, 191.
[18] K. Frank, T. Wolff, H. Lorenz, A. Seidel-Morgenstern, Y. Suchorski, M. Piorkowska, H. Weiss, *J. Catal.* **2007**, *247*, 176.
[19] M. Havecker, A. Knop-Gericke, H. Bluhm, E. Kleimenov, R. W. Mayer, M. Fait, R. Schlögl, *Appl. Surf. Sci.* **2004**, *230*, 272.
[20] S. Albonetti, F. Cavani, F. Trifiro, *Catal. Rev.* **1996**, *38*, 413.
[21] I. E. Wachs, B. M. Weckhuysen, *Appl. Catal. A* **1997**, *157*, 67.
[22] G. Deo, I. E. Wachs, J. Haber, *Crit. Rev. Surf. Chem.* **1994**, *4*, 141.
[23] G. J. Hutchings, J. A. Lopez-Sanchez, J. K. Bartley, J. M. Webster, A. Burrows, C. J. Kiely, A. F. Carley, C. Rhodes, M. Hävecker, A. Knop-Gericke, R. W. Mayer, R. Schlögl, J. C. Volta, M. Poliakoff, *J. Catal.* **2002**, *208*, 197.
[24] C. J. Kiely, S. Sajip, I. J. Ellison, M. T. Sananes, G. J. Hutchings, J. C. Volta, *Catal. Lett.* **1995**, *33*, 357.

[25] J. A. Lopez-Sanchez, J. K. Bartley, A. Burrows, C. J. Kiely, M. Hävecker, R. Schlögl, J. C. Volta, M. Poliakoff, G. J. Hutchings, *New J. Chem.* **2002**, *26*, 1811.
[26] A. C. Dupuis, M. Abu Haija, B. Richter, H. Kuhlenbeck, H. J. Freund, *Surf. Sci.* **2003**, *539*, 99.
[27] H. Niehus, R. P. Blum, D. Ahlbehrendt, *Surf. Rev. Lett.* **2003**, *10*, 353.
[28] I. Czekaj, K. Hermann, M. Witko, *Surf. Sci.* **2003**, *545*, 85.
[29] G. Kresse, S. Surnev, J. Schoiswohl, F. P. Netzer, *Surf. Sci.* **2004**, *555*, 118.
[30] J. Schoiswohl, M. Sock, S. Surnev, M. G. Ramsey, F. P. Netzer, G. Kresse, J. N. Andersen, *Surf. Sci.* **2004**, *555*, 101.
[31] P. Mars, D. W. van Krevelen, *Chem. Eng. Sci.* **1954**, *Suppl.3*, 41.
[32] K. Devriendt, H. Poelman, L. Fiermans, *Surf. Sci.* **1999**, *433*, 734.
[33] E. A. Colbourn, *Surf. Sci. Rep.* **1992**, *15*, 281.
[34] a) K. W. Urban, *MRS Bull.* **2007**, *32*, 946; b) D. S. Su, T. Jacob, T. W. Hansen, D. Wang, R. Schlögl, B. Freitag, S. Kujawa, *Angew. Chem.* **2008**, *120*, 5083; *Angew. Chem. Int. Ed.* **2008**, *47*, 5005.
[35] S. C. Street, C. Xu, D. W. Goodman, *Annu. Rev. Phys. Chem.* **1997**, *48*, 43.
[36] C. L. Jia, L. Houben, K. Urban, *Philos. Mag. Lett.* **2006**, *86*, 683.
[37] C. L. Jia, V. Nagarajan, J. Q. He, L. Houben, T. Zhao, R. Ramesh, K. Urban, R. Waser, *Nat. Mater.* **2007**, *6*, 64.
[38] K. W. Urban, *Science* **2008**, *321*, 506.
[39] V. E. Henrich, P. A. Cox, *The Surface Science of Metal Oxides*, Cambridge University Press, Cambridge, **1994**.
[40] N. Erdman, K. R. Poeppelmeier, M. Asta, O. Warschkow, D. E. Ellis, L. D. Marks, *Nature* **2002**, *419*, 55.
[41] J. Goniakowski, F. Finocchi, C. Noguera, *Rep. Prog. Phys.* **2008**, *71*, 016501.
[42] J. B. Wagner, S. B. Abd Hamid, D. Othman, O. Timpe, S. Knobl, D. Niemeyer, D. S. Su, R. Schlögl, *J. Catal.* **2004**, *225*, 78.
[43] J. B. Wagner, O. Timpe, F. A. Hamid, A. Trunschke, U. Wild, D. S. Su, R. K. Widi, S. B. Abd Hamid, R. Schlögl, *Top. Catal.* **2006**, *38*, 51.
[44] T. Ushikubo, H. Nakamura, Y. Koyasu, S. Wajiki, U.S. Patent 5 380 933, **1995**.
[45] H. Tsuji, Y. Koyasu, *J. Am. Chem. Soc.* **2002**, *124*, 5608.
[46] F. Wang, W. Ueda, *Chem. Commun.* **2009**, 1079.
[47] P. DeSanto, D. J. Buttrey, R. K. Grasselli, C. G. Lugmair, A. F. Volpe, B. H. Toby, T. Vogt, *Z. Kristallogr.* **2004**, *219*, 152.
[48] W. D. Pyrz, D. A. Blom, T. Vogt, D. J. Buttrey, *Angew. Chem.* **2008**, *120*, 2830; *Angew. Chem. Int. Ed.* **2008**, *47*, 2788.
[49] N. R. Shiju,, X. H. Liang, A. W. Weimer, C. D. Liang, S. Dai, V. V. Guliants, *J. Am. Chem. Soc.* **2008**, *130*, 5850.
[50] A. C. Sanfiz, T. W. Hansen, A. Sakthivel, A. Trunschke, R. Schlögl, A. Knoester, H. H. Brongersma, M. H. Looi, S. B. A. Hamid, *J. Catal.* **2008**, *258*, 35.
[51] M. A. Henderson, *Surf. Sci.* **1994**, *319*, 315.
[52] W. Ueda, D. Vitry, T. Katou, *Catal. Today* **2004**, *96*, 235.
[53] R. K. Grasselli, *Catal. Today* **2005**, *99*, 23.
[54] W. Ueda, K. Oshihara, *Appl. Catal. A* **2000**, *200*, 135.
[55] V. V. Guliants, R. Bhandari, H. H. Brongersma, A. Knoester, A. M. Gaffney, S. A. Han, *J. Phys. Chem. B* **2005**, *109*, 10234.
[56] J. Holmberg, S. Hansen, R. K. Grasselli, A. Andersson, *Top. Catal.* **2006**, *38*, 17.

